Androgen deprivation triggers a cytokine signaling switch to induce immune suppression and prostate cancer recurrence

Kai Sha[1,6,8], Renyuan Zhang[1,6,9], Aerken Maolake[1], Shalini Singh[1,10], Gurkamal Chatta[4], Kevin H. Eng[1,2,11], Kent L. Nastiuk[1,3,5,7] and John J. Krolewski[1,5,7]

Departments of [1]Cancer Genetics and Genomics, [2]Biostatistics and Bioinformatics, [3]Urology and [4]Medicine, Roswell Park Comprehensive Cancer Center, Buffalo, NY 14263

[5]Department of Biology and Program in Data Science and Analytics, Buffalo State University/ SUNY, Buffalo, NY 14222

[6,7]These authors contributed equally to this report

[8]Current address: LabCorp-Monogram Biosciences, South San Francisco, CA 95080
[9]Current address: Thermo-Fisher Scientific, Ann Arbor, MI 48104
[10]Current address: BiologyWorks, Los Angeles, CA 90004
[11]Current address: Eikon Therapeutics, Jersey City, NJ 07302

CORRESPONDENCE:

Dr. J.J. Krolewski, Buffalo State University/ SUNY, Department of Biology; 1300 Elmwood Avenue; Buffalo, NY 14222; krolewjj@buffalostate.edu; 949-872-9107

Dr. K.L. Nastiuk, Roswell Park Comprehensive Cancer Center, Department of Cancer Genetics and Genomics, Elm & High Streets, Buffalo, NY 14263; kent.nastiuk@roswellpark.org; 716-845-5771

KEY WORDS: androgen deprivation, tumor stem cell, CCL2, immunosuppression, resistance, TNF
CONFLICT OF INTEREST: The authors declare that there are no potential conflicts of interest
FINANCIAL SUPPORT: This work was supported by the Department of Defense Prostate Cancer Research Program No. W81XWH-19-1-0378 (to J.J. Krolewski and K.L. Nastiuk), institutional funds from the Roswell Park Alliance Foundation and the National Cancer Institute Cancer Center Support Grant P30-CA016056 to Roswell Park Comprehensive Cancer Center.

ABSTRACT

Androgen deprivation therapy (ADT) is an effective but not curative treatment for advanced and recurrent prostate cancer (PC). We investigated the mechanisms controlling the response to androgen-deprivation by surgical castration in genetically-engineered mouse models (GEMMs) of PC, using high frequency ultrasound imaging to rigorously measure tumor volume. Castration initially causes almost all tumors to shrink in volume, but many tumors subsequently recur within 5-10 weeks. Blockade of tumor necrosis factor (TNF) signaling a few days in advance of castration surgery, using a TNFR2 ligand trap, prevents regression in a PTEN-deficient GEMM. Following tumor regression, a stem cell-like population within the tumor increases along with TNF protein levels. Tumor cell lines in culture recapitulate these *in vivo* observations, suggesting the possibility that stem cells are the source of TNF. When TNF signaling blockade is administered immediately prior to castration, tumors regress but recurrence is prevented. This implies that a late wave of TNF secretion within the tumor – which coincides with the expression of NFκB regulated genes – drives recurrence. The inhibition of signaling downstream of an NFκB-regulated protein – chemokine C-C motif ligand 2 (CCL2) – prevents post-castration tumor recurrence, phenocopying post-castration (late) TNF signaling blockade. CCL2 was originally identified as a macrophage chemoattractant and indeed at late times after castration gene sets related to chemotaxis and migration are up-regulated. Importantly, enhanced CCL2 signaling during the tumor recurrence phase coincides with an increase in pro-tumorigenic macrophages and a decrease in CD8 T cells, suggesting that recurrence is driven at least in part by tumor immunosuppression. In summary, we demonstrate that a therapy-induced switch in TNF signaling induces an immunosuppressive tumor microenvironment and concomitant tumor recurrence.

55 **INTRODUCTION**

56 Androgen deprivation therapy (ADT) via surgical castration (1) and currently via medical therapy
57 employing gonadotropin releasing hormone analogues (2), has been an effective treatment for advanced
58 primary and recurrent prostate cancer (PC) for many decades. Within the past several years, the addition
59 of either the microtubule toxin docetaxel or the androgen biosynthesis inhibitor abiraterone to ADT has
60 improved the medical therapy (3). However, these ADT-combination therapies have only marginally
61 extended overall survival and the fundamental issue for patients with advanced primary and recurrent
62 PC remains the same: ADT (or an ADT-combination) rarely cures PC and resistant tumors are eventually
63 lethal. Thus, there is a need to develop additional therapies for PC, preferably by identifying molecular
64 targets that are mechanistically linked to the development of ADT resistance. ADT is effective because
65 the growth of almost every prostate cancer is dependent on a program of gene expression mediated by
66 the androgen receptor and a set of critical co-regulators. The androgen receptor (AR) gene is activated
67 by genetic alteration in only a small fraction of primary PCs (4). Instead, one or two alterations of a small
68 group of other genes (5) is sufficient to re-program the AR cistrome to transcribe a set of genes that
69 promote immortalization and tumorigenesis (6). Additional alterations in a second class of genes driving
70 proliferation and growth – such as the PTEN tumor suppressor or the c-MYC oncogene – completes the
71 process of transformation to prostate cancer (5).

72 Tissue reconstitution studies (7) have shown that androgen blockade can act indirectly via soluble
73 factors derived from the tumor micro-environment (TME). Consistent with this paradigm, in which
74 proteins are secreted into the TME and act on the cell of origin (autocrine) or on other cells within the
75 TME (paracrine), we have previously investigated the response of prostate cancers to androgen
76 deprivation (8-13), using cell culture and murine models of human prostate cancer. A recurrent theme of
77 this research has been the role of tumor necrosis factor (TNF) as a pleotropic signaling mediator within
78 the PC TME. TNF binds and trimerizes its cognate receptor and signals via a complex network of
79 intercellular protein-protein interactions to promote either an anti-tumor or pro-tumor fate, depending on
80 the cellular context. In this report, we examine the role of TNF and TNF-regulated genes in the response

81 to castration in a genetically engineered mouse model (GEMM) of PC driven by deletion of the PTEN
82 gene (14). Castration induces regression and subsequent recurrence in this GEMM, resembling the
83 onset of castration resistant prostate cancer (CRPC). Both responses are dependent on TNF signaling
84 and can be separately blocked by differentially timing the administration of a TNF ligand trap molecule.
85 At late times post-castration, when the tumor is beginning to recur in a castration resistant form, TNF
86 induces NFκB-mediated gene expression. Moreover, we demonstrate that the NFκB-induced gene
87 CCL2 – which encodes a protein that is chemotactic for immune suppressive cells such as tumor
88 associated macrophages (TAMs) – is necessary for recurrence in the PTEN-loss model as well as in a
89 second GEMM of PC that is driven by MYC over-expression. Thus, a TNF signaling switch induces
90 immunosuppression in the tumor microenvironment to promote castration-resistant tumor recurrence.
91

92 **MATERIALS AND METHODS**

93 **Animals and tumor imaging**

94 All animal studies were approved by the Roswell Park Comprehensive Cancer Center (RPCCC)
95 institutional animal care and use committee. Male Pb-Cre4; PTEN$^{fl/fl}$ mice (14) and Hi-MYC (15) were
96 breed in the RPCCC laboratory animal shared resource. Mice were housed in environmentally-controlled
97 conditions on a 12-hour light/dark cycle with water and food. For both genetically engineered mouse
98 models (GEMMs) we studied, male pups were genotyped and tumor volumes were monitored by three-
99 dimensional high frequency ultrasound (HFUS) imaging, as previously described (9,16). In brief, mice
100 were anesthetized, the abdomen was depilated and B-mode image scans were acquired using a Vevo
101 2100 micro-ultrasound imaging system (Vevo LAZR; VisualSonics Inc., Toronto). Images were imported
102 into Amira software (Visualization Sciences Group, Burlington, MA) for 3D tumor reconstruction and
103 volume determination. Tumors developed in ~100% of male animals for both GEMMs. The histology,
104 lobular location and usual age to reach 300-500 mm^3 volume are provided for the two models in
105 Supplementary Table S1. Mice with tumor volumes of 300-500 mm^3 were randomly enrolled into
106 experimental groups, and surgically castrated (or sham-operated) via scrotal incision, under isoflurane

107 anesthesia (17). To systematically define the response of the GEMMs to castration, we applied a murine
108 approximation of the human clinical RECIST (response evaluation criteria in solid tumors) criteria (18).
109 Thus, we define regression as a volume decline of 16% or more post-castration and recurrence (of tumors
110 that had met the regression standard) as occurring when we observe volume increases of 11% from the
111 volume nadir, in at least two temporally distinct imaging sessions. Etanercept (sTNFR2-Fc; Amgen,
112 Thousand Oaks, CA, USA) was injected intra-peritoneally (4mg/kg) twice per week for up to 5 weeks
113 following castration, based on our previous studies (8,11). The CCR2 antagonist (CCR2a) BMS-741672
114 (Torcis Bioscience, Bristol, UK) was injected intraperitoneally (2 mg/kg) three times per week as
115 described (19), beginning one day prior to castration.

116 **Tumor tissue collection and processing**

117 After mice were sacrificed, individual prostate tumors were identified grossly, excised and cut in half.
118 Typically, a portion was flash frozen in liquid nitrogen and stored in a liquid nitrogen freezer while a
119 second portion was fixed in paraformaldehyde at room temperature overnight, washed in PBS, stored at
120 4°C and embedded in paraffin as required for the preparation of tissue sections. Mouse prostate tumor
121 and normal tissues were dissociated for single cell RNA sequencing using the Tumor Dissociation kits
122 from Miltenyi Biotec (cat. no. 130-096-730). Briefly, tissue was excised, washed with chilled 1x PBS,
123 placed in a petri dish on ice, cut into 2-4 mm^3 pieces, transferred to a gentleMACS C tube (cat. no. 130-
124 096-334) containing DMEM/enzyme mix and then attached to gentleMACS Octo Dissociator (cat. no.
125 130-096-427) with heating running the '37C_m_TDK_1' (mouse) program. The suspension was filtered
126 through a 40 µm cell strainer (Falcon). The cells were harvested by centrifugation at 400g for 10 min and
127 resuspended in chilled 1X Red Blood Cell Removal Solution (Miltenyi Biotec, cat. no.130-094-183).
128 Debris was then removed using the Debris Removal Solution (Miltenyi Biotec, cat. no. 130-109-398)
129 following the manufacturer's instructions.

130 **Cell culture**

131 The C4-2 cell line, from Jer-Tsong Hsieh, UT Southwestern Medical Center, Dallas, TX, was used to
132 model castration-resistant prostate cancer (20). C4-2 was periodically monitored by polymerase chain

133 reaction (PCR) for mycoplasma contamination (21) and DNA fingerprinting was employed to authenticate
134 this cell lines (22). C4-2 was cultured in RPMI-1640 media supplemented with 10% FCS and 1%
135 penicillin/streptomycin. Enzalutamide was from Selleck Chemicals (Houston, TX).

136 **Enzyme-linked immunosorbent assays (ELISA)**

137 In the case of prostate tumors, tissue powder was homogenized in NP-40 buffer using Sonic
138 Dismembrator (Fisher Scientific, Hampton, NH) at power 7 for 30 sec. The supernatant was collected by
139 centrifugation and stored at −80°C for subsequent analysis. In the case of cell culture, cells were seeded
140 at a density of 0.8-1×10^5/ml as mono-cultures and media stored at 4°C was used for subsequent analysis.
141 TNF and CCL2 were quantitated by ELISA (eBioscience, San Diego, CA), according to the
142 manufacturer's instructions. Protein concentration was determined using bicinchoninic acid reagent
143 (Pierce, ThermoFisher Scientific), according to the manufacturer's instructions.

144 **Fluorescent activating cell sorting**

145 Cells in culture were detached from cell culture plasticware using StemPro accutase (Gibco,
146 Gaithersburg, MD), washed with PBS and incubated with 1% BSA in 1x PBS for 10 min at 4°C. Human
147 cell lines were incubated with antibodies against CD166-FITC (3A6; Ancell, Stillwater, MN; 1:1250) and
148 CD49f-Alexa Fluor® 647 (GoH3; Biolegend, San Diego, CA; 1:200) for 30 min at 4°C. Mouse prostates
149 were disaggregated using 1mg/ml type I collagenase and 1mg/ml Dispase (Invitrogen, Carlsbad, CA) in
150 RPMI medium and filtered through 40 μm cell strainer. Cells were suspended in DMEM with 10% FBS
151 and 1% L-glutamine, and then incubated with fluor-labeled antibodies for 30 min at 4°C. Mouse cells
152 were incubated with antibodies against Sca-1-APC (D7; 1:500), CD49f-PE (GoH3; 1:333), and the
153 'lineage' markers (Ter119-FITC (TER-119; 1:250), CD31-FITC (390; 1:250) and CD45-FITC (30-F11;
154 1:250)). LSC FACS, first gating on lineage-negative (Lin^-) cells and then CD49f and SCA-1 was
155 performed as described by Witte and colleagues (23). All anti-mouse antibodies were purchased from
156 eBioscience (San Diego, CA). 7-AAD (Invitrogen, Carlsbad, CA; 1:1000) was used to determine dead
157 cells. FACS analysis was performed using the BD LSR-II (BD Bioscience, San Jose, CA) and analyzed

158 by Winlist 3D (Version 8.0; Verity Software House, Topsham, ME, USA). Cell sorting was done by BD
159 FACSAria-II (BD Bioscience, San Jose, CA).

160 **Colony formation assay**

161 Cells were seeded in 6-well plates at densities of 0.5×10^3, 1×10^3 and 1.5×10^3 cells per well and
162 cultured for 21 days. The media was removed, wells were washed once with PBS, stained with 2%
163 toluidine blue for 30 min and scanned with Epson Perfection 1240U (Suwa, Nagano Prefecture, Japan).
164 Colonies were imaged and then enumerated using ImageJ.

165 **Immunohistochemistry**

166 Immunohistochemical (IHC) staining was performed on 5 μm sections of formalin fixed paraffin-
167 embedded (FFPE) mouse prostate tumor tissue. Sections were incubated with monoclonal antibodies
168 against F4/80 (BM8; Biolegend, San Diego, CA, USA; 1:600), CD8alpha (D4W2Z; Cell Signaling
169 Technology, Danvers, MA, USA; 1:400), or CCL2 (2H5; Biolegend, San Diego, CA, USA; 1:100),
170 appropriate horse-radish peroxide secondary antibodies and reacted with 3,3-diaminobenzidine using an
171 automated tissue processor. IHC and H&E images were captured at 20x magnification using Olympus
172 BX45 microscope and cellSens software (Olympus, Shinjuku-ku, Tokyo, Japan). Ten random high
173 powered (200X) fields were captured for each section and were blinded prior to quantitation of stained
174 cells ($F4/80^+$ or $CCL2^+$ macrophages or $CD8a^+$ lymphocytes) using ImageJ.

175 **RNA extraction, sequencing and analysis**

176 RNA was extracted from liquid nitrogen frozen tumor samples by pulverizing tissue into a powder using
177 a pre-cooled mortar and pestle. TRIzol (Invitrogen, Carlsbad, CA) was then added by a ratio of 1 mL of
178 TRIzol per 100 mg of tumor tissue, and RNA extraction completed as per manufacturer's instructions
179 (24). Bulk RNA-seq data processing and analysis was performed as follows. FastQC v0.11.5 was used
180 for quality control; STAR v2.6.0a (25) was employed to align the reads to the murine reference genome
181 (GRCm38 M16) and gene expression was then quantified using RSEM (26). FastQC, RSEM, STAR
182 were all performed in a local Linux/Unix computing environment. Subsequent analyses were performed
183 using the following R-software packages from the Bioconductor website. Estimated gene counts from

184 RSEM were filtered and the upper quartile was normalized using edgeR (27). Differential gene
185 expression (DGE) was performed using Limma after Voom transformation followed by linear regression
186 (28,29). The significance threshold was set to false discovery rate (FDR) / adjusted p-value of less than
187 0.05 with a fold change greater than 2 (FDR < 0.05 and |log2 fold change| > 1). Sets of genes with
188 FDR<0.05 and |log2FC| from the DGE analysis were subjected to Gene Ontology analysis of biological
189 processes as described (30), using the website tool (http://pantherdb.org/index.jsp). Heatmaps were
190 generated using the package Complexheatmap (31). Single cell gene expression libraries were
191 generated using the 10X Genomics Chromium platform and sequenced on a NovaSeq 6000 (Illumina).
192 Processing of scRNA-seq data was performed as follows. For QC, normalization, clustering and
193 differential gene expression, the Cellranger v6.0.0 software (https://support.10xgenomics.com/single-
194 cell-geneexpression/software/) was used to align FASTQ sequencing reads to the mm10 (mouse)
195 reference transcriptome, generating single cell feature counts for each sample. Count data from all cells
196 were included in a 'SingleCellExperiment' (version 1.8.0) object (32). The 'scater' package (version
197 1.14.5) was used to filter cells and normalize counts per million (CPM) (33). Transcripts from a given cell
198 were removed from the analysis if the corresponding transcriptome met any of the following criteria: 20%
199 or more reads aligned to mitochondrial genes, 1000 total counts per cell or less, or 300 genes per cell or
200 less. The dimensionality of this transcriptomic data was reduced using the t-distributed stochastic
201 neighbor embedding (t-SNE) algorithm (34,35). The 'limma' package (29) was used to identify
202 differentially expressed genes to refine the assignment of clusters generated by the t-SNE algorithm.

203 **Statistics**

204 Data are presented as the mean ± SEM. Statistical analyses were conducted using JMP-Pro12 (SAS,
205 Cary, NC, USA). Differences between two means was assessed by Student's unpaired *t*-test and
206 differences among multiple means by one-way or two-way ANOVA followed by Tukey-Kramer HSD post-
207 hoc testing if the F-statistic was significant. For the small *n*, categorical data sets related to the studies
208 using GEM prostate cancer models shown in Figures 4A, 5C and 5D, we employed the exact binomial

209 test to determine the Clopper-Pearson confidence interval for the proportion and Fisher's exact test to
210 determine the *p*-values. Supplementary Table S3 summarizes these statistical analyses.

211 **RESULTS**

212 **Tumor recurrence following castration-induced regression in PTEN-deficient PC**

213 Mice engineered to delete the PTEN gene in the prostate epithelium at puberty uniformly develop an
214 intraductal form of prostate adenocarcinoma (14) (Table S1). To investigate the response of prostate
215 cancer to androgen deprivation therapies, we used high frequency ultrasound (HFUS) and three-
216 dimension reconstruction software (9,16) to serially determine the volume of tumors in live animals (Fig.
217 1A). As seen in Figure 1B, the kinetics of tumor volume following castration is complex. Immediately
218 following castration, tumor volume continues to increase similar to the non-castrated control. We recently
219 demonstrated that this delay in tumor regression – which is not observed in the normal murine prostate
220 – is driven by glucocorticoid receptor signaling transiently substituting for tumor-specific re-programmed
221 AR signaling (9). Following this delay, the tumors regressed as expected but within ~5 weeks most
222 began to increase in volume, implying tumor recurrence and mimicking the development of CRPC in
223 men. Regression and recurrence events were defined by adapting standard human oncology imaging
224 protocols to mice, as described in the MATERIALS AND METHODS section and in the legend to
225 Supplementary Table S2. Serial HFUS imaging of a large cohort castrated PTEN-deficient mice
226 (including those in Fig. 1) is summarized in Supplementary Table S2, demonstrating 40-80% recurrence
227 dependent on the period of post-castration observation.

228 We measured TNF protein levels in tumor lysates, and found an increase at 5 weeks post-castration,
229 when tumor recurrence is beginning (Fig. 1C). Previously, we had observed an increase in *Tnf* mRNA
230 at 8 hours post-castration in the stromal compartment of the normal prostate, suggesting a relatively
231 direct effect of androgen-withdrawal on TNF expression (11). In the case of PTEN-deficient tumors, the
232 increase in TNF protein at a late time post-castration suggests a more complex transcriptional and/or
233 translational regulatory mechanism in response to androgen withdrawal. Alternately, the increase in TNF
234 at late times post-castration might be due to the expansion of a population of TNF-expressing cells as

235 the tumor evolves in response to androgen deprivation. We queried gene expression profiles in public
236 databases from two previously published studies of men who had either hormone-naïve PC or CRPC
237 (36,37), to gain insight into this question. Increased *TNF* mRNA expression in CRPC, relative to
238 castration-naive primary PC, correlated with elevated expression of stem cell-related genes in both
239 datasets (Fig. S1).

240 **Androgen-deprivation induced TNF secretion is due to increased basal cell stemness**

241 To determine if we could detect a change in the stem cell-like tumor epithelial cell populations as the
242 tumors began to increase in volume following castration-induced regression, we examined single cell
243 preparations from tumors for cell surface expression of stem cell markers, using fluorescent-activated
244 cell sorting (FACS). We observed an increase in $Lin^-/Sca1^+/CD49f^{hi}$ (LSC^{hi}) cells at 25 days post-
245 castration, relative to non-castrated tumors (Fig 1D). These cells correspond to the cytokeratin-$5^+/p63^+$
246 basal stem cell population (38), a multipotent stem cell population that is required for the post-natal
247 development of the prostate (39). Basal stem cells are distinct from $Lin^-/Sca1^+/CD49f^{med}$ (LSC^{med}) luminal
248 progenitor cells (identified in the lower right population in Fig. 1D) that are the likely tumor initiating cell
249 populations for most human prostate cancers (39,40).

250 The data in Figures 1 and S1 suggest that the TNF secreted during the post-castration recurrence
251 phase in the PTEN-deficient tumors might be derived from a cell population with increased levels of
252 'stemness'. To test this more thoroughly, we performed experiments using the C4-2 and LNCaP cell
253 culture models of PC. First, we observed that long-term culture in the anti-androgen enzalutamide (41)
254 significantly reduced the growth rate of C4-2 prostate cancer cells (Fig. 2A), as expected. Reduced
255 growth was accompanied by an increase in the fraction of cells that resembled basal stem cells (Fig. 2B-
256 C) and a coordinate increased in TNF levels (Fig. 2C). In the analyses for Figure 2, we employed CD166
257 as a basal stemness biomarker (42). We also performed the enzalutamide selection experiment on the
258 LNCaP cell line, an isogenic parental line for C4-2 (20), which is more androgen-responsive (Fig S2A).
259 We observed a similar correlation between stemness and TNF secretion (Fig. S2B-C). Finally, we
260 replicated enzalutamide selection for both C4-2 and LNCaP cell lines, using immunofluorescence

261 microscopy to identify CD49f^{hi} and CD166^{hi} cells (Fig. S3). Again, an increase in the fraction of cells
262 scoring for these stemness markers correlated with increased TNF secretion. Stem cell marker
263 enrichment >10% was typically required to detect an increase in TNF in the media of enzalutamide-
264 treated cultures. Next, we treated C4-2 cells with enzalutamide for 20 days and used preparative FACS
265 to partially purified cells into CD166^{lo} and CD166^{hi} fractions (Fig. 3A). TNF levels were higher in
266 conditioned media from the CD166^{hi} fraction relative to the CD166^{lo} fraction (Fig. 3B). We also
267 demonstrated that the efficiency of colony formation – a functional marker of stemness – correlated with
268 the level of expression of CD166 (Fig. 3C).

269 **Differentially-timed blockade of TNF signaling**

270 We previously employed cell culture and mouse models of prostate cancer to demonstrate that TNF
271 signaling mediates two distinct responses to ADT – an anti-tumorigenic apoptotic/regression phenotype
272 (8,43) and a pro-tumorigenic cell migration phenotype (44). Given the observations in Figure 1, we
273 hypothesized that TNF mediates both the regression and recurrence phases that occur after castration
274 (Fig. 1B). To test this, we treated tumor-bearing mice with etanercept – a sTNFR2-Fc fusion protein,
275 which competitively binds TNF (45) and prevents receptor binding – beginning at three distinct time
276 points: three days prior, one day prior, and three days following castration. When etanercept is
277 administered three days before castration (Fig. 4A, -3d), castration-induced regression is blocked, and
278 tumor growth is similar to the sham group (Fig. 1B). Etanercept given one day before castration does
279 not affect regression but blocks recurrence (Fig. 4A, -1d). Finally, when etanercept was administered
280 three days after castration there is no detectable effect on regression or recurrence (Fig. 4A, +3d).
281 Instead, the result resembles castration alone (Fig. 1B).

282 To gain insight into the nature of the different molecular processes occurring during regression
283 and recurrence, we performed gene set enrichment analysis (GSEA) on RNA sequence data from bulk
284 tumor mRNA. Specifically, we compared samples from sham castrated mice with those from either mice
285 six days after castration (Fig. 4B, upper panel) or mice 35 days after castration (Fig. 4B, lower panel).
286 Multiple gene sets related to TNF-induced transcription, most NFkB-related, were uniformly down-

287 regulated at six days post-castration but up-regulated 5 weeks after castration, relative to the sham
288 conditions. The switch in TNF-related gene sets from down-regulation to up-regulation is consistent with
289 a switch from apoptosis signaling (low NFkB levels) to signaling that promotes transcription of NFkB-
290 regulated genes (high NFkB levels).

291 **CCL2 signaling is required for recurrence in murine prostate cancer models**

292 CCL2 is a chemotactic cytokine (chemokine) (46) linked to prostate cancer pathogenesis (47). The
293 CCL2-CCR2 signaling axis has multiple pro-tumorigenic functions, most notably the recruitment and
294 polarization of tumor associated macrophages (TAMs) (48). Previously we demonstrated autocrine
295 CCL2 secretion following enzalutamide induction of TNF in mono-cultures of C4-2 cells (10), consistent
296 with CCL2 gene transcription via TNF induction of NFκB (49). We returned to the enzalutamide selection
297 experiments shown in Figure 2C and Supplementary Figure S2 and found that the secretion of CCL2
298 protein increased over time, in a manner dependent on secreted TNF, in enzalutamide treated C4-2 and
299 LNCaP cells (Fig. S4A-B)To assess paracrine CCL2 production in response to androgen deprivation, we
300 replicated these experiments using co-cultures of LNCaP or C4-2 plus the myofibroblast-like WPMY-1
301 cell line (50), grown in enzalutamide-containing media. Again, we observed coordinate secretion of TNF
302 and CCL2 (Fig. S4C). Co-cultures produced 5- to 20-fold more CCL2 than the prostate cancer cell line
303 mono-cultures. We also found that enzalutamide-treated co-cultures of C4-2 plus WPMY-1 produced
304 conditioned media that induced migration of THP-1, a $CCR2^{+}$ macrophage-like leukemia cell line that is
305 a model for TAMs (Fig. S4D).

306 These observations suggested that paracrine TNF induction of CCL2 in the prostate cancer TME
307 might be responsible for tumor recurrence at late times post-castration, possibly by recruiting
308 immunosuppressive TAMs (51). Indeed, we found that in the samples from Figure 1C, CCL2 increased
309 at 5 weeks (Fig. 5A), coincident with the rise in TNF that accompanies tumor recurrence. Tissue sections
310 corresponding to tumors 5 weeks post-castration showed an increase in stroma-localized macrophage-
311 like cells expressing CCL2 (Fig. 5B). Moreover, CCL2 expression was reduced in tumor tissue sections
312 from castrated mice that received etanercept, consistent with CCL2 regulation by TNF (Fig. 5B). To

313 determine if CCL2 signaling was necessary for post-castration tumor recurrence in prostate cancer
314 mouse models, mice bearing PTEN-deficient prostate cancers received an antagonist of CCR2 prior to
315 castration. Serial imaging revealed that none of the tumors met the criteria for recurrence (Fig. 5C),
316 indicating that CCL2-CCR2 signaling is indeed required for castration resistant recurrence in this model.
317 Importantly, the tumor kinetics produced by CCR2 blockade phenocopies the effect of etanercept
318 administered one-day prior to castration (Fig. 4A, -1d), consistent with TNF regulation of CCL2 gene
319 transcription via NFkB. To confirm the role of CCL2 signaling we replicated the CCR2 inhibition studies
320 in the Hi-MYC prostate cancer GEMM, which has a similar response to castration (regression delay,
321 regression then recurrence) as the PTEN-deficient GEMM (Fig. 5D, blue symbols; see also ref. (9)). We
322 observed that CCR2a treatment prior to castration was comparably effective at preventing post-castration
323 recurrence in Hi-MYC mice (Fig. 5D, red symbols; also see Fig. S5).

324 We used a transcriptomic approach to further investigate CCL2 signaling, immune cell migration,
325 and TAMs in the development of castration-resistant prostate cancer in the PTEN-deficient GEMM.
326 Differential gene expression (DGE) analysis was performed on bulk RNA-sequencing data from tumor
327 tissue and genes with FDR<0.05 and |log2FC| (see Fig. S6 and details in the legend) were subjected to
328 Gene Ontology (GO) enrichment analysis (Fig. 6). These analyses revealed that a very similar category
329 of gene sets – mediating immune cell chemotaxis and migration – are up-regulated in the bulk tumor
330 mRNA from mice 35 days post-castration (Fig. 6A) but are down-regulated in the bulk tumor mRNA from
331 mice 35 days post-castration which were treated with CCR2a (Fig. 6B). We also assembled a TAM-
332 related gene set and found that these genes are similarly regulated: 'up' in the 35 days post-castration
333 group and 'down' in the 35 days post-castrated group treated with CCR2a (Fig. 6C).

334 **An immunosuppressive cell profile is induced in the TME during recurrence**

335 Taken together, the analyses in Figures 5 and 6 indicate that CCL2 might be functioning to recruit TAMs
336 and drive the progression to, or recurrence as, castration resistant prostate cancer (52). Thus, to
337 determine how TNF-CCL2 signaling effects the tumor immune microenvironment in the PTEN-deficient
338 murine prostate cancer model, we used immunohistochemistry (IHC) to quantitate F4/80- and CD8-

339 stained cells in tissue sections from the tumors. As seen in Figure 7A, F4/80-stained cells (presumptive
340 TAMs) increase, most notably at 35 days post-castration, just as tumor re-growth in the recurrence phase
341 is beginning and CCL2 levels are peaking (Fig. 5A). In addition, etanercept partially blocks this increase
342 in TAMs and coordinately inhibits tumor recurrence. CD8 T cells (presumptive cytolytic T-lymphocytes;
343 CTLs) decreased over time following castration and this was also partially reversed by etanercept
344 administration to the mice bearing PTEN-deficient tumors. Figure 7B demonstrates that blocking CCL2
345 signaling with the CCR2 antagonist has the expected effect – it reduces F4/80-stained cells and
346 increased CD8-stained cells, reversing the castration-induced immunosuppressive cell profile and
347 coordinately preventing prostate cancer recurrence (Fig. 5C). Integrating the data on F4/80-staining,
348 CD8-staining and CCL2 ELISAs for tumors treated and harvested at various times post-castration reveals
349 a demonstrates a high degree of correlation of the key immune components we examined. Specifically,
350 there is positive correlation of macrophages and CCL2 secretion and a negative correlation of T cells
351 with macrophage as well as with CCL2 section (Fig. S7). We also observed a more pronounced CD45+
352 cell infiltrate in the recurrent tumors, relative to non-recurrent tumors (Fig. S7B).

353 **Transcriptomic CD8/CD68 ratio predicts castration outcome**

354 Next, we carried out transcriptomic profiling to confirm the IHC studies in Figure 7, which correlated an
355 immunosuppressive immune cell profile (elevated CD68, reduced CD8) with recurrence of the PTEN-
356 deficient tumor. Specifically, three mice bearing PTEN-deficient prostate cancers were castrated and
357 tumor volume was HFUS-monitored for 42 days (Fig. 8A). One mouse failed to regress and was labeled
358 'stable'. Two mice regressed, one of which showed recurrence 21 days after castration. We recovered
359 the tumors, and performed single cell RNA sequencing. Transcript count data was pooled and tSNE
360 dimensionality reduction was used, along with subjective cell annotation, to identify six cell populations
361 (Fig. 8B). Among CD45-positive immune cells, TAMs were identified as those cells expressing both
362 CD68 and CD80, while cytolytic T cells (CTL) were defined as those expressing CD3 and CD8 (see
363 details in the legend to Fig. 8). In Figure 8C, we plotted the ratio of CTL to TAM, and observed that

364 compared with the regressing tumor, the recurrent tumor had a lower CTL/TAM ratio. This is consistent
365 with the IHC analysis in Figure 7A and suggests that immune suppression drives tumor re-growth.
366

367 **DISCUSSION**

368 **TNF signaling switch**

369 Employing a HFUS-based imaging protocol to measure tumor volume in live mice, we are able to resolve
370 the response of genetically-engineered murine prostate cancers to castration into multiple,
371 mechanistically-distinct phases, as illustrated for the PTEN-deficient prostate cancer model in Figure 1
372 (the kinetics for the castration response in the Hi-MYC GEMM are similar). Immediately following
373 castration, there is an increase in tumor volume in both prostate cancer GEMMs. We recently
374 demonstrated that this seemingly paradoxical effect is dependent on glucocorticoid signaling transiently
375 substituting for tumor-specific androgen receptor signals that are blocked by the androgen ablative effects
376 of castration (9). After 4-7 days of gradually increasing volume, the tumors begin to regress due to
377 apoptotic cell death of the epithelial tumor cells in the cancerous glands, consistent with the classical
378 morphological description of apoptosis (53). In addition to tumor epithelial cell apoptosis, there is a loss
379 of vascular integrity within the tumor that contributes to the regression phase (54,55). Some tumors
380 continue to regress for more than two months, but for the majority – up to 75% of individual tumors in the
381 prostate cancer GEMMs we studied – recurrence begins 4-6 weeks after castration (Fig. 1A, Fig 4D and
382 Supplementary Table S2b).

383 We sought to decipher the intra- and inter-cellular signaling events that occur within the tumor
384 and the surrounding microenvironment in response to androgen deprivation (castration). Previously we
385 had shown that TNF – but not other common death receptor ligands (FasL and TRAIL) – is necessary
386 for apoptosis-driven regression of the normal murine prostate (11). In addition, we also found that TNF
387 is required for so-called vascular regression of murine prostate cancers, probably by triggering
388 endothelial cell apoptosis (8). The loss of vascular integrity leads to tumor hypoxia within a day following
389 castration. While these events occur multiple days prior to the onset of a measurable reduction in
390 prostate cancer volume, hypoxia may indirectly drive regression by inducing tumor epithelial cell
391 apoptosis via TP53 (8). In the current studies, when we administered etanercept to PTEN-deficient mice
392 three days prior to castration, regression was effectively inhibited (Fig. 4A and Supplementary Table

393 S2a). This observation is consistent with TNF-driven apoptosis of tumor epithelial and endothelial cells.
394 The increase in TNF protein 5 weeks post-castration (Fig. 1C) – at a point when most tumors
395 have regressed – suggested a second role for TNF signaling in the response to androgen deprivation.
396 Indeed, blockade of TNF signaling beginning one day prior to castration results in most tumors
397 regressing, but no recurrence (Fig. 4A and Supplementary Table S2a). Thus, TNF signaling switches
398 from pro-apoptotic signaling that activates caspase-8 and drives regression to pro-tumorigenic signaling
399 that activates the NFκB and/or PI3K/Akt pathways, promoting tumor cell survival and proliferation and
400 tumor recurrence. The results of transcriptional analysis (Fig. 4B) support the switch to a pro-tumorigenic
401 phenotype: we observed increased expression of NFκB-related gene sets in bulk mRNA recovered from
402 tumor samples at 35 days, versus 6 days, post-castration. A key consequence of NFκB signaling during
403 the recurrence phase is the induction of CCL2 protein levels 35 days post-castration (Fig. 5A). Moreover,
404 the administration of a CCR2 antagonist to tumor bearing mice prevented castration-induced recurrence
405 (Fig. 5C), phenocopying the effects of -1d TNF blockade by etanercept treatment (Fig. 4A, -1d panel).
406 This observation is consistent with CCL2 expression downstream of TNF-NFκB signaling. Similarly, the
407 number of CCL2-staining cells in the TME was reduced in tumors from mice receiving etanercept to block
408 TNF signaling (Fig. 5B).

409 **Increased tumor cell stemness following androgen deprivation drives pro-tumor TNF signaling**

410 While the pleotropic signaling effects of TNF are well-established, an important mechanistic question in
411 the context of this report is whether changes in the tumor and surrounding TME are responsible for the
412 post-castration switch in TNF signaling. Two potential determinants are the spatial and temporal pattern
413 of TNF production/ secretion and the context of the cells that TNF signaling targets. Previously, we
414 showed that in the normal rat prostate TNF mRNA and protein increased as early as 8 hours post-
415 castration, with the most significant increase occurring within the stromal compartment of the prostate
416 (11). However, in PTEN-deficient murine tumors there is no discernable increase in TNF protein in the
417 first 24 hours post-castration (Fig. 1B). Alternatively, death receptor driven apoptosis can be triggered
418 by down-regulation of the CASP8 inhibitor CFLAR (56). Indeed, we previously found castration reduced

419 CFLAR expression within 12 hours post-castration in the normal rat prostate (12,13). Moreover, CFLAR
420 protein is up-regulated in CRPC patient samples (57). To investigate the mechanism of the late (5 weeks
421 post-castration) increase in TNF, we blocked AR action with enzalutamide in prostate cancer cell culture
422 models (10). After 3 weeks of culture in enzalutamide, TNF secretion and stemness were increased in
423 both C42 and LNCaP cell lines (Figs. 2 and Supplementary Figs. S2-S3). Higher levels of TNF secretion
424 occurred in cultures enriched for expression of one of the stem cell-like markers (Fig. 3). The increased
425 expression of stem cell-like genes following androgen deprivation may reflect the death of luminal-like
426 cells (low stemness) and selection for, or expansion of, basal-like cells (higher stemness) that have
427 increased levels of NFκB and therefore secrete more TNF protein. We observed an increase in basal
428 stem-like cells at 25 days post-castration in the PTEN-deficient tumor model (Fig. 1D), suggesting a
429 similar phenomenon is occurring *in vivo*. It is also possible that the increase in stemness that we observe
430 post-castration is due to lineage plasticity of pre-existing cells, rather than selection and expansion of
431 *bone fide* tumor stem cells (58). Regardless, it appears most likely that the increase in TNF secretion
432 observed 5 weeks post-castration is a consequence of changes in cellular context rather than a
433 promoter/enhancer-driven transcriptional response.

434 **Immune suppression is a key consequence of increased tumor cell stemness**

435 By investigating the switch in TNF signaling, we identified CCL2 secretion as a key TNF-NFκB-induced
436 event required for the onset of tumor recurrence in the PTEN-deficient GEMM (Fig. 5). Moreover, CCL2
437 is also required for recurrence in the genetically distinct Hi-MYC GEMM, suggesting CCL2 may be a
438 common driver for recurrence post-castration, at least in murine models of prostate cancer. Although
439 CCL2 has multiple pro-tumorigenic immune-modulating functions in prostate and other cancers (59), the
440 transcriptomic studies described in Figure 6 are consistent with TAM recruitment. Specifically, Gene
441 Ontology analysis (Fig. 6A-B) indicates that CCL2 induces immune cell chemotaxis and migration at the
442 time of recurrence, which is the behavior expected of TAMs as well as other myeloid immune suppressive
443 cells, such as myeloid-derived suppressor cells (MDSC). The heat map in Figure 6C showed up-
444 regulation of TAM-related genes, while IHC analysis in Figure 7 (and Supplementary Fig. S7)

445 demonstrated a coordinate increase in F4/80+ macrophages and CCL2 at the time of recurrence. The
446 latter two observations support a critical role for TAMs, but do not rule out a role for MDSC. Identifying
447 the precise tumor immune cell populations within the TME that modulate the response of cancers to
448 therapy is the focus of considerable ongoing research (60). TAMs are a heterogenous set of immune
449 cells which are predominantly pro-tumorigenic (61) and have been implicated in human and murine
450 prostate cancers (62,63). Although an oversimplification of the immune response to cancer, a balance
451 between anti-tumor cytolytic T cells and immunosuppressive myeloid cell populations may predict the
452 success of emerging immunotherapies. Indeed, variants of the CTL/TAM ratio – similar to our
453 observations in Figures 7 and 8 – are potential prognostic biomarkers in patients with melanoma (64),
454 breast cancer (65) and hepatocellular carcinoma (66). **Prospective: a model for the development of**
455 **CRPC**

456 The models we employed are anatomically similar to non-metastatic CRPC (nmCRPC) in that the tumor
457 is localized to the prostate, whereas in metastatic CRPC (mCRPC) the TME is derived from the metastatic
458 site, such as bone. Most CRPC is discovered clinically as mCRPC and indeed nmCRPC is likely a
459 transient state that progresses to mCRPC (67). Castration of mice bearing PTEN-deficient or Hi-MYC
460 prostate cancers induces regression and then recurrence – a pattern very similar to that seen in the
461 development of human CRPC. Importantly, HFUS imaging provides real-time volume data to ensure that
462 the complex kinetics of tumor volume changes can be used to accurately categorize the response of
463 each tumor to androgen deprivation. Supplementary Figure S8 is a mechanistic model consistent with
464 our findings. It proposes that TNF secretion into the TME first drives regression and subsequently
465 induces an immunosuppressive state that leads to recurrence. The specific signal may vary depending
466 on the TME context. For example, in some PTEN-deficient GEMMs, IL1ß triggers myeloid immune
467 suppression (68). Most of our analyses were performed on bulk tumor tissue – this represents a
468 significant limitation of the studies in this report. Future studies employing multi-modal single cell
469 analyses will be critical to elucidating the molecular interactions between tumor cells and the
470 myofibroblasts, endothelial cells and immune cells that constitute the TME. These studies are underway

471 in our laboratories. Although the CCL2 antagonist was effective at preventing recurrence in our GEMMs,
472 a monoclonal antibody which binds CCL2 failed in a phase 2 patient trial in mCRPC (69). This may have
473 been due to technical issues with the drug (69), or possibly heterogeneity among human CRPCs. Indeed,
474 Giancotti and colleagues identified three subtypes of CRPC (70) and proposed that one of these –
475 mesenchymal stem-like prostate cancer – might use CCL2 signaling to promote myeloid immune
476 suppression. Thus, in the future patients with this CRPC subtype may be candidates for anti-CCL2
477 therapies.
478

479 **ACKNOWLEDGEMENTS**

480 We acknowledge: Chawnshang Chang and Shu-Yuan Yeh (University of Rochester) for encouraging us
481 to investigate the pro-tumorigenic role of CCL2 in prostate cancer; Yvonne Saenger (Albert Einstein
482 College of Medicine) for helpful discussions on the ratio of CTLs and TAMs in tumor immune suppression,
483 Bo Xu (Roswell Park Comprehensive Cancer Center) for discussions on the histopathology of murine
484 prostate cancers and Michalis Mastri (Thermo-Fisher/ GIBCO) for assistance with computational analysis
485 of RNA sequence data.
486

REFERENCES

1. Huggins C, Hodges CV (1941) Studies on prostatic cancer. I. The effect of castration, of estrogen and of androgen injection on serum phosphatases in metastatic carcinoma of the prostate. Cancer Res 1:293-297.

2. Labrie F, Belanger A, Luu-The V, Labrie C, Simard J, Cusan L, Gomez J, Candas B (2005) Gonadotropin-releasing hormone agonists in the treatment of prostate cancer. Endocr Rev 26:361-379.

3. Sartor O, de Bono JS (2018) Metastatic Prostate Cancer. N Engl J Med 378:645-657.

4. Cancer Genome Atlas Research Network. Electronic address scmo, Cancer Genome Atlas Research N (2015) The Molecular Taxonomy of Primary Prostate Cancer. Cell 163:1011-1025.

5. Copeland BT, Pal SK, Bolton EC, Jones JO (2018) The androgen receptor malignancy shift in prostate cancer. Prostate 78:521-531.

6. Grbesa I, Augello MA, Liu D, McNally DR, Gaffney CD, Huang D, Lin K, Ivenitsky D, Goueli R, Robinson BD, Khani F, Deonarine LD, Blattner M, Elemento O, Davicioni E, Sboner A, Barbieri CE (2021) Reshaping of the androgen-driven chromatin landscape in normal prostate cells by early cancer drivers and effect on therapeutic sensitivity. Cell Reports 36:109625.

7. Cunha GR, Hayward SW, Wang YZ, Ricke WA (2003) Role of the stromal microenvironment in carcinogenesis of the prostate. Int J Cancer 107:1-10.

8. Krolewski JJ, Singh S, Sha K, Jaiswal N, Turowski SG, Pan C, Rich LJ, Seshadri M, Nastiuk KL (2022) TNF signaling is required for castration-induced vascular damage preceding prostate cancer regression. Cancers 14:6020.

9. Maolake A, Zhang R, Sha K, Singh S, Pan C, Xu B, Chatta G, Eng KH, Nastiuk KL, Krolewski JJ (2021) Glucocorticoid signaling delays castration-induced regression in murine models of prostate cancer. bioRxiv doi.org/10.1101/2021.10.11.463722.

10. Sha K, Yeh S, Chang C, Nastiuk K, Krolewski JJ (2015) TNF signaling mediates an enzalutamide-induced metastatic phenotype of prostate cancer and microenvironment cell co-cultures. Oncotarget 6:25726-25740.

11. Davis JS, Nastiuk KL, Krolewski JJ (2011) TNF is necessary for castration-induced prostate regression, whereas TRAIL and FasL are dispensable. Mol Endocrinol 25:611-620.

12. Nastiuk KL, Kim JW, Mann M, Krolewski JJ (2003) Androgen regulation of FLICE-like inhibitory protein gene expression in the rat prostate. J Cell Physiol 196:386-393.

13. Cornforth AN, Davis JS, Khanifar E, Nastiuk KL, Krolewski JJ (2008) FOXO3a mediates the androgen-dependent regulation of FLIP and contributes to TRAIL-induced apoptosis of LNCaP cells. Oncogene 27:4422-4433.

14. Wang S, Gao J, Lei Q, Rozengurt N, Pritchard C, Jiao J, Thomas GV, Li G, Roy-Burman P, Nelson PS, Liu X, Wu H (2003) Prostate-specific deletion of the murine Pten tumor suppressor gene leads to metastatic prostate cancer. Cancer Cell 4:209-221.

538 15. Ellwood-Yen K, Wongvipat J, Sawyers C (2006) Transgenic mouse model for rapid
539 pharmacodynamic evaluation of antiandrogens. Cancer Res 66:10513-10516.
540
541 16. Singh S, Pan C, Wood R, Yeh C-R, Yeh S, Sha K, Krolewski JJ, Nastiuk KL (2015) Quantitative
542 volumetric imaging of normal, neoplastic and hyperplastic mouse prostate using ultrasound. BMC
543 Urol 15:97.
544
545 17. Pan C, Jaiswal Agrawal N, Zulia Y, Singh S, Sha K, Mohler JL, Eng KH, Chakkalakal JV, Krolewski
546 JJ, Nastiuk KL (2020) Prostate tumor-derived GDF11 accelerates androgen deprivation therapy-
547 induced sarcopenia. JCI Insight 5:e127018.
548
549 18. Schwartz LH, Litiere S, de Vries E, Ford R, Gwyther S, Mandrekar S, Shankar L, Bogaerts J, Chen
550 A, Dancey J, Hayes W, Hodi FS, Hoekstra OS, Huang EP, Lin N, Liu Y, Therasse P, Wolchok JD,
551 Seymour L (2016) RECIST 1.1-Update and clarification: From the RECIST committee. Eur J Cancer
552 62:132-137.
553
554 19. Macanas-Pirard P, Quezada T, Navarrete L, Broekhuizen R, Leisewitz A, Nervi B, Ramirez PA
555 (2017) The CCL2/CCR2 Axis Affects Transmigration and Proliferation but Not Resistance to
556 Chemotherapy of Acute Myeloid Leukemia Cells. PLoS One 12:e0168888.
557
558 20. Thalmann GN, Anezinis PE, Chang SM, Zhau HE, Kim EE, Hopwood VL, Pathak S, von Eschenbach
559 AC, Chung LW (1994) Androgen-independent cancer progression and bone metastasis in the
560 LNCaP model of human prostate cancer. Cancer Res 54:2577-2581.
561
562 21. Pruckler JM, Pruckler JM, Ades E (1995) Detection by polymerase chain reaction of all common
563 *mycoplasma* in a cell culture facility. Pathobiol 63:9-11.
564
565 22. Dirks WG, Drexler HG (2005) Authentication of scientific human cell lines: easy-to-use DNA
566 fingerprinting. Methods Mol Biol 290:35-50.
567
568 23. Lukacs RU, Goldstein AS, Lawson DA, Cheng D, Witte ON (2010) Isolation, cultivation and
569 characterization of adult murine prostate stem cells. Nat Protoc 5:702-713.
570
571 24. Chougoni KK, Grossman SR (2020) Extraction of high-quality RNA from mouse pancreatic tumors.
572 MethodsX 7:101163.
573
574 25. Dobin A, Davis CA, Schlesinger F, Drenkow J, Zaleski C, Jha S, Batut P, Chaisson M, Gingeras TR
575 (2013) STAR: ultrafast universal RNA-seq aligner. Bioinformatics 29:15-21.
576
577 26. Li B, Dewey CN (2011) RSEM: accurate transcript quantification from RNA-Seq data with or without
578 a reference genome. BMC Bioinformatics 12:323.
579
580 27. Robinson MD, McCarthy DJ, Smyth GK (2010) edgeR: a Bioconductor package for differential
581 expression analysis of digital gene expression data. Bioinformatics 26:139-140.
582
583 28. Law CW, Chen Y, Shi W, Smyth GK (2014) voom: Precision weights unlock linear model analysis
584 tools for RNA-seq read counts. Genome Biol 15:R29.
585
586 29. Ritchie ME, Phipson B, Wu D, Hu Y, Law CW, Shi W, Smyth GK (2015) limma powers differential
587 expression analyses for RNA-sequencing and microarray studies. Nucleic Acids Res 43:e47.
588

30. Ashburner M, Ball CA, Blake JA, Botstein D, Butler H, Cherry JM, Davis AP, Dolinski K, Dwight SS, Eppig JT, Harris MA, Hill DP, Issel-Tarver L, Kasarskis A, Lewis S, Matese JC, Richardson JE, Ringwald M, Rubin GM, Sherlock G (2000) Gene ontology: tool for the unification of biology. The Gene Ontology Consortium. Nat Genet 25:25-29.

31. Gu Z, Eils R, Schlesner M (2016) Complex heatmaps reveal patterns and correlations in multidimensional genomic data. Bioinformatics 32:2847-2849.

32. Amezquita RA, Lun ATL, Becht E, Carey VJ, Carpp LN, Geistlinger L, Marini F, Rue-Albrecht K, Risso D, Soneson C, Waldron L, Pages H, Smith ML, Huber W, Morgan M, Gottardo R, Hicks SC (2020) Orchestrating single-cell analysis with Bioconductor. Nat Methods 17:137-145.

33. McCarthy DJ, Campbell KR, Lun AT, Wills QF (2017) Scater: pre-processing, quality control, normalization and visualization of single-cell RNA-seq data in R. Bioinformatics 33:1179-1186.

34. Kobak D, Berens P (2019) The art of using t-SNE for single-cell transcriptomics. Nat Commun 10:5416.

35. Zhou B, Jin W (2020) Visualization of Single Cell RNA-Seq Data Using t-SNE in R. Methods Mol Biol 2117:159-167.

36. Yu YP, Landsittel D, Jing L, Nelson J, Ren B, Liu L, McDonald C, Thomas R, Dhir R, Finkelstein S, Michalopoulos G, Becich M, Luo JH (2004) Gene expression alterations in prostate cancer predicting tumor aggression and preceding development of malignancy. J Clin Oncol 22:2790-2799.

37. Ross-Adams H, Lamb AD, Dunning MJ, Halim S, Lindberg J, Massie CM, Egevad LA, Russell R, Ramos-Montoya A, Vowler SL, Sharma NL, Kay J, Whitaker H, Clark J, Hurst R, Gnanapragasam VJ, Shah NC, Warren AY, Cooper CS, Lynch AG, Stark R, Mills IG, Gronberg H, Neal DE, CamCa PSG (2015) Integration of copy number and transcriptomics provides risk stratification in prostate cancer: A discovery and validation cohort study. EBioMedicine 2:1133-1144.

38. Lawson DA, Xin L, Lukacs RU, Cheng D, Witte ON (2007) Isolation and functional characterization of murine prostate stem cells. Proc Natl Acad Sci U S A 104:181-186.

39. Sackmann Sala L, Boutillon F, Menara G, De Goyon-Pelard A, Leprevost M, Codzamanian J, Lister N, Pencik J, Clark A, Cagnard N, Bole-Feysot C, Moriggl R, Risbridger GP, Taylor RA, Kenner L, Guidotti JE, Goffin V (2017) A rare castration-resistant progenitor cell population is highly enriched in Pten-null prostate tumours. J Pathol 243:51-64.

40. Wang ZA, Toivanen R, Bergren SK, Chambon P, Shen MM (2014) Luminal Cells Are Favored as the Cell of Origin for Prostate Cancer. Cell Reports 8:1339-1346.

41. Schalken J, Fitzpatrick JM (2016) Enzalutamide: targeting the androgen signalling pathway in metastatic castration-resistant prostate cancer. BJU Int 117:215-225.

42. Mulholland DJ, Kobayashi N, Ruscetti M, Zhi A, Tran LM, Huang J, Gleave M, Wu H (2012) Pten loss and RAS/MAPK activation cooperate to promote EMT and metastasis initiated from prostate cancer stem/progenitor cells. Cancer Res 72:1878-1889.

43. Davis JS, Nastiuk KL, Krolewski JJ (2011) TNF is necessary for castration-induced prostate regression, whereas TRAIL and FasL are dispensable. Mol Endocrinol 25:611-620.

641 44. Sha K, Yeh S, Chang C, Nastiuk KL, Krolewski JJ (2015) TNF signaling mediates an enzalutamide-
642 induced metastatic phenotype of prostate cancer and microenvironment cell co-cultures. Oncotarget
643 6:25726-25740.
644
645 45. Kaymakcalan Z, Sakorafas P, Bose S, Scesney S, Xiong L, Hanzatian DK, Salfeld J, Sasso EH
646 (2009) Comparisons of affinities, avidities, and complement activation of adalimumab, infliximab,
647 and etanercept in binding to soluble and membrane tumor necrosis factor. Clin Immunol 131:308-
648 316.
649
650 46. Matsushima K, Larsen CG, DuBois GC, Oppenheim JJ (1989) Purification and characterization of a
651 novel monocyte chemotactic and activating factor produced by a human myelomonocytic cell line. J
652 Exp Med 169:1485-1490.
653
654 47. Zhang J, Patel L, Pienta KJ (2010) CC chemokine ligand 2 (CCL2) promotes prostate cancer
655 tumorigenesis and metastasis. Cytokine Growth Factor Rev 21:41-48.
656
657 48. Fei L, Ren X, Yu H, Zhan Y (2021) Targeting the CCL2/CCR2 Axis in Cancer Immunotherapy: One
658 Stone, Three Birds? Front Immunol 12:771210.
659
660 49. Jin F, Li Y, Dixon JR, Selvaraj S, Ye Z, Lee AY, Yen CA, Schmitt AD, Espinoza CA, Ren B (2013) A
661 high-resolution map of the three-dimensional chromatin interactome in human cells. Nature 503:290-
662 294.
663
664 50. Webber MM, Trakul N, Thraves PS, Bello-DeOcampo D, Chu WW, Storto PD, Huard TK, Rhim JS,
665 Williams DE (1999) A human prostatic stromal myofibroblast cell line WPMY-1: a model for stromal-
666 epithelial interactions in prostatic neoplasia. Carcinogenesis 20:1185-1192.
667
668 51. Larionova I, Tuguzbaeva G, Ponomaryova A, Stakheyeva M, Cherdyntseva N, Pavlov V,
669 Choinzonov E, Kzhyshkowska J (2020) Tumor-associated macrophages in human breast,
670 colorectal, lung, ovarian and prostate cancers. Frontiers Oncology 10:566511.
671
672 52. Loberg RD, Ying C, Craig M, Yan L, Snyder LA, Pienta KJ (2007) CCL2 as an important mediator of
673 prostate cancer growth in vivo through the regulation of macrophage infiltration. Neoplasia 9:556-
674 562.
675
676 53. Kerr JF, Wyllie AH, Currie AR (1972) Apoptosis: a basic biological phenomenon with wide-ranging
677 implications in tissue kinetics. Br J Cancer 26:239-257.
678
679 54. Godoy A, Montecinos VP, Gray DR, Sotomayor P, Yau JM, Vethanayagam RR, Singh S, Mohler JL,
680 Smith GJ (2011) Androgen deprivation induces rapid involution and recovery of human prostate
681 vasculature. Am J Physiol Endocrinol Metab 300:E263-275.
682
683 55. Buttyan R, Ghafar MA, Shabsigh A (2000) The effects of androgen deprivation on the prostate gland:
684 cell death mediated by vascular regression. Curr Opin Urol 10:415-420.
685
686 56. Irmler M, Thome M, Hahne M, Schneider P, Hofmann K, Steiner V, Bodmer J-L, Schröter M, Burns
687 K, Mattmann C, Rimoldi D, French LE, Tschopp J (1997) Inhibition of death receptor signals by
688 cellular FLIP. Nature 388:190-195.
689
690 57. McCourt C, Maxwell P, Mazzucchelli R, Montironi R, Scarpelli M, Salto-Tellez M, O'Sullivan JM,
691 Longley DB, Waugh DJ (2012) Elevation of c-FLIP in castrate-resistant prostate cancer antagonizes
692 therapeutic response to androgen receptor-targeted therapy. Clin Cancer Res 18:3822-3833.

58. Sandhu HS, Portman KL, Zhou X, Zhao J, Rialdi A, Sfakianos JP, Guccione E, Kyprianou N, Zhang B, Mulholland DJ (2022) Dynamic plasticity of prostate cancer intermediate cells during androgen receptor-targeted therapy. Cell Reports 40:111123.

59. Hao Q, Vadgama JV, Wang P (2020) CCL2/CCR2 signaling in cancer pathogenesis. Cell communication and signaling 18:82.

60. Mellman I, Chen DS, Powles T, Turley SJ (2023) The cancer-immunity cycle: Indication, genotype, and immunotype. Immunity 56:2188-2205.

61. Kloosterman DJ, Akkari L (2023) Macrophages at the interface of the co-evolving cancer ecosystem. Cell 186:1627-1651.

62. Gollapudi K, Galet C, Grogan T, Zhang H, Said JW, Huang J, Elashoff D, Freedland SJ, Rettig M, Aronson WJ (2013) Association between tumor-associated macrophage infiltration, high grade prostate cancer, and biochemical recurrence after radical prostatectomy. Am J Cancer Res 3:523-529.

63. Escamilla J, Schokrpur S, Liu C, Priceman SJ, Moughon D, Jiang Z, Pouliot F, Magyar C, Sung JL, Xu J, Deng G, West BL, Bollag G, Fradet Y, Lacombe L, Jung ME, Huang J, Wu L (2015) CSF1 receptor targeting in prostate cancer reverses macrophage-mediated resistance to androgen blockade therapy. Cancer Res 75:950-962.

64. Gartrell-Corrado RD, Chen AX, Rizk EM, Marks DK, Bogardus MH, Hart TD, Silverman AM, Bayan CY, Finkel GG, Barker LW, Komatsubara KM, Carvajal RD, Horst BA, Chang R, Monod A, Rabadan R, Saenger YM (2020) Linking Transcriptomic and Imaging Data Defines Features of a Favorable Tumor Immune Microenvironment and Identifies a Combination Biomarker for Primary Melanoma. Cancer Res 80:1078-1087.

65. DeNardo DG, Brennan DJ, Rexhepaj E, Ruffell B, Shiao SL, Madden SF, Gallagher WM, Wadhwani N, Keil SD, Junaid SA, Rugo HS, Hwang ES, Jirstrom K, West BL, Coussens LM (2011) Leukocyte complexity predicts breast cancer survival and functionally regulates response to chemotherapy. Cancer Discov 1:54-67.

66. Xin H, Liang D, Zhang M, Ren D, Chen H, Zhang H, Li S, Ding G, Zhang C, Ding Z, Wu L, Han W, Zhou W, Chen Y, Luo H, Wang Y, Zhang H, Liu S, Li N (2021) The CD68+ macrophages to CD8+ T-cell ratio is associated with clinical outcomes in hepatitis B virus (HBV)-related hepatocellular carcinoma. HPB 23:1061-1071.

67. Figueiredo A, Costa L, Mauricio MJ, Figueira L, Ramos R, Martins-da-Silva C (2022) Nonmetastatic Castration-Resistant Prostate Cancer: Current Challenges and Trends. Clin Drug Investig 42:631-642.

68. Wang D, Cheng C, Chen X, Wang J, Liu K, Jing N, Xu P, Xi X, Sun Y, Ji Z, Zhao H, He Y, Zhang K, Du X, Dong B, Fang Y, Zhang P, Qian X, Xue W, Gao WQ, Zhu HH (2023) IL-1beta Is an Androgen-Responsive Target in Macrophages for Immunotherapy of Prostate Cancer. Adv Sci (Weinh) 10:e2206889.

69. Pienta KJ, Machiels JP, Schrijvers D, Alekseev B, Shkolnik M, Crabb SJ, Li S, Seetharam S, Puchalski TA, Takimoto C, Elsayed Y, Dawkins F, de Bono JS (2013) Phase 2 study of carlumab (CNTO 888), a human monoclonal antibody against CC-chemokine ligand 2 (CCL2), in metastatic castration-resistant prostate cancer. Investigational new drugs Invest New Drugs 31:760-768.

745 70. Su W, Han HH, Wang Y, Zhang B, Zhou B, Cheng Y, Rumandla A, Gurrapu S, Chakraborty G, Su
746 J, Yang G, Liang X, Wang G, Rosen N, Scher HI, Ouerfelli O, Giancotti FG (2019) The Polycomb
747 Repressor Complex 1 Drives Double-Negative Prostate Cancer Metastasis by Coordinating
748 Stemness and Immune Suppression. Cancer Cell 36:139-155 e110.
749
750 71. Horoszewicz JS, Leong SS, Kawinski E, Karr JP, Rosenthal H, Chu TM, Mirand EA, Murphy GP
751 (1983) LNCaP model of human prostatic carcinoma. Cancer Res 43:1809-1818.
752
753 72. Tsuchiya S, Yamabe M, Yamaguchi Y, Kobayashi Y, Konno T, Tada K (1980) Establishment and
754 characterization of a human acute monocytic leukemia cell line (THP-1). Int J Cancer 26:171-176.
755
756 73. Arefieva TI, Kukhtina NB, Antonova OA, Krasnikova TL (2005) MCP-1-stimulated chemotaxis of
757 monocytic and endothelial cells is dependent on activation of different signaling cascades. Cytokine
758 31:439-446.
759
760 74. Franklin RA, Liao W, Sarkar A, Kim MV, Bivona MR, Liu K, Pamer EG, Li MO (2014) The cellular
761 and molecular origin of tumor-associated macrophages. Science 344:921-925.
762
763

FIGURE 1

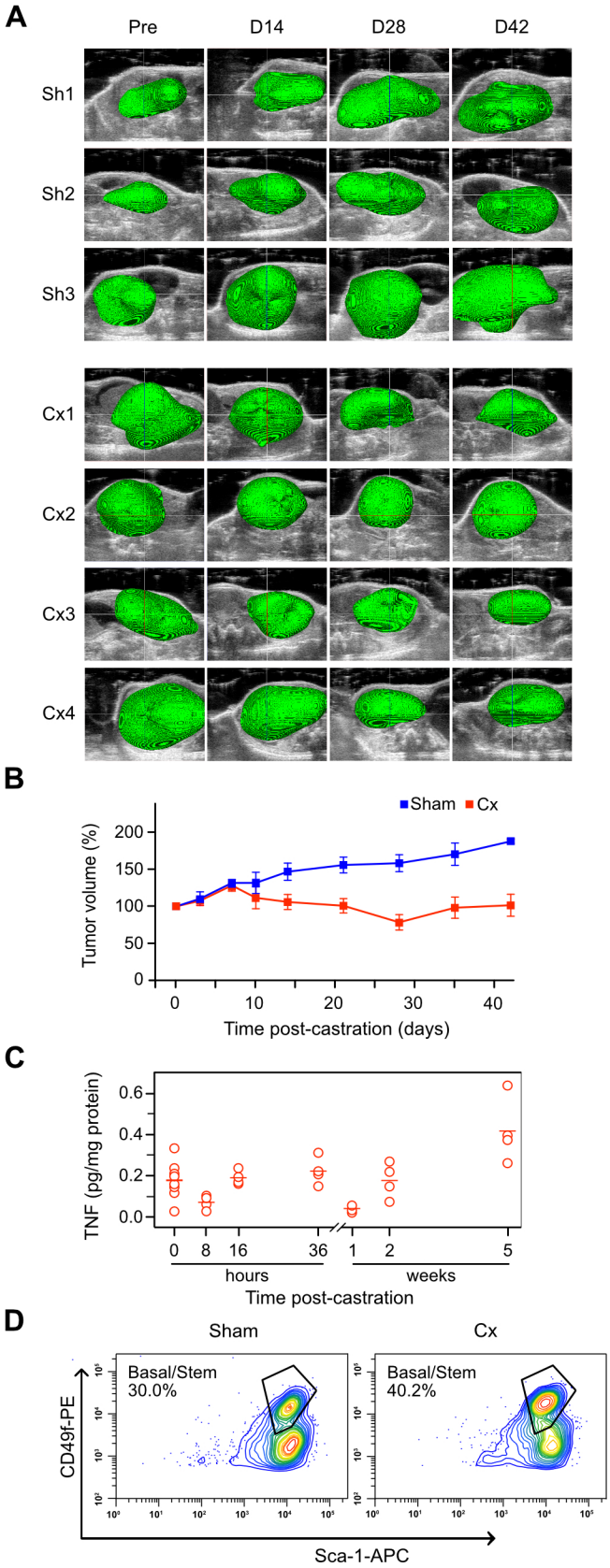

Figure 1. Castration induces tumor recurrence, and an increase in TNF and stemness in prostate tumors from PTEN-deficient mice. Mice bearing PTEN-deficient tumors were either castrated (Cx1-4) or sham-operated (Sh1-3) and serially imaged using HFUS. In some cases, tumor tissue was recovered for further analysis. **A**. 3D reconstruction of tumor-bearing ventral lobes (pseudo-colored green) performed as described in Materials & Methods. **B**. Tumor volume kinetics post-castration. Tumor volume was determined from HFUS images using Amira software. Mean tumor volume at the indicated times post-castration (n=4, red) or post-sham operation (n=3, blue) is shown as percent pre-castration volume (mean [%] ± SEM). **C**. TNF levels in tumors tissue extracts were measured by ELISA and normalized to total protein in the tissue sample, at the indicated times post castration. One-way ANOVA followed by Tukey-Kramer HSD test revealed a difference in TNF levels between 0 and 5 weeks ($p<0.01$). **D**. LSC FACS analysis of tumor cells from sham (left) and castrated (Cx; right) PTEN-deficient mice. Tumors were disaggregated and cells were processed for Lin^-/Sca-1/CD49f FACS analysis (23). Relative fluorescence intensities are shown as contour plots. The LSC^{hi} population is labeled 'Basal/stem'. The population in the lower right quadrant (LSC^{med}) corresponds to luminal progenitors. A representative analysis is shown. Sham LSC FACS was replicated 5 times (mean[%]±SEM = 27.0±4.0); 25d post-castration LSC FACS was replicated 4 times (mean[%]±SEM = 38.2±1.7). Student's t-test revealed a difference between Sham and Cx in the LSC^{hi} population ($p<0.05$).

FIGURE 2

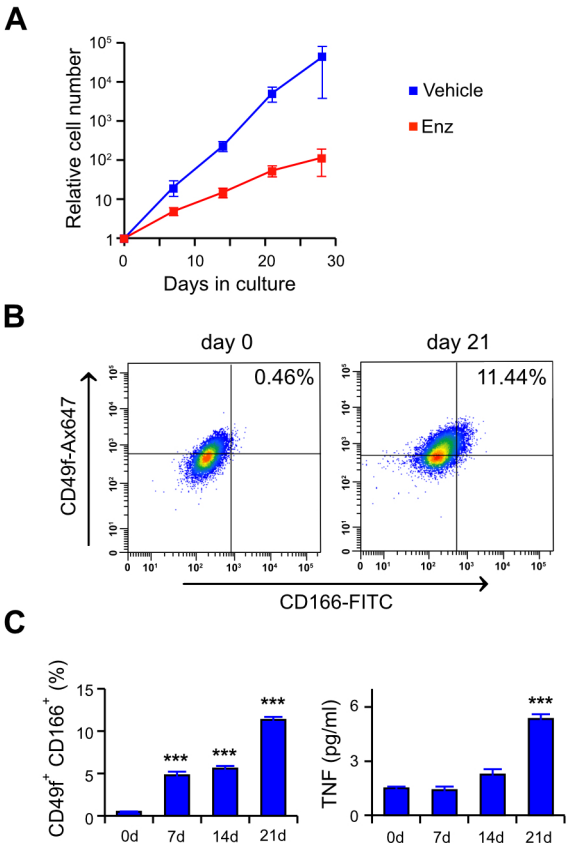

Figure 2. Extended enzalutamide treatment selects for basal stemness and TNF secretion. C4-2 cells were grown in media plus 10% serum and treated with vehicle (blue) or 10 μM enzalutamide (Enz; red) for the indicated time. **A.** C4-2 cell growth curve in the presence of enzalutamide. Trypan-blue excluding live cells were counted microscopically at the indicated times. Data are shown as mean ± s.e.m. (n=3). Two-way ANOVA followed by Tukey-Kramer HSD test revealed a difference in cell number for the Enz treated culture at 28d versus 0d (p<0.01). **B.** FACS analysis for basal cell stemness markers in enzalutamide treated C4-2 cells. Cells grown in enzalutamide for the indicated time, were incubated with the fluor-labeled antibodies, analyzed by FACS and relative fluorescence intensity represented as dot plots. The fraction of the cells that correspond to the $CD49f^{hi}/CD166^{hi}$ population (upper, right quadrant) is indicated. Additional time points are in Supplementary Figure S2. **C.** Fraction of cells scoring $CD49f^{hi}/CD166^{hi}$ and corresponding TNF secretion, at the indicated time of culture in media plus enzalutamide. Data from FACS analyses (see Fig. S2) is plotted on the left and TNF levels in the media determined by ELISA is plotted on the right. Values are given as mean ± s.e.m. (n = 2). **, p < 0.01 ***p < 0.001 (two-way ANOVA followed by Tukey-Kramer HSD test).

FIGURE 3

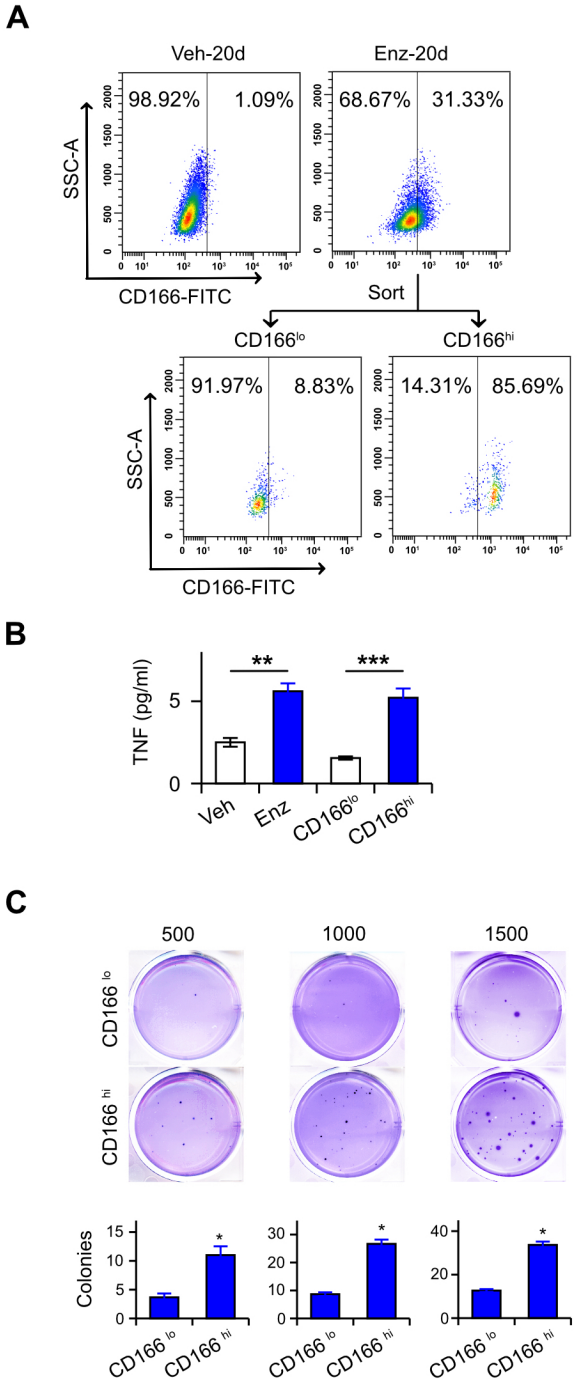

Figure 3. Enzalutamide treatment selects for a TNF-expressing basal stem cell population. C4-2 cells were grown for 20 days in media plus 10% serum containing 10 μM enzalutamide, enriched for CD166^{hi} expression. ELISA was used to measure TNF and colony formation. **A.** CD166-enrichment was performed via FACS to sort CD166^{hi} and CD166^{lo} C4-2 cells treated as indicated. The purity of the unsorted and sorted CD166^{hi} and CD166^{lo} populations are shown. **B.** TNF secretion of the indicated cultures (left to right): unsorted, vehicle-treated (veh); unsorted, enzalutamide-treated (enz); and sorted, enzalutamide-treated (CD166^{lo}, CD166^{hi}). TNF measured by ELISA, and plotted as mean ± s.e.m. (n=3). **p<0.01, ***p<0.001 (One-way ANOVA followed by Tukey-Kramer HSD test). **C.** Colony formation assay of enriched CD166^{hi} and CD166^{lo} cell populations sorted as in **A**. Seeding densities were 500, 1000, and 1500 cells/well, respectively. Colony counts per well are plotted. *p<0.05 (Student's unpaired t-test).

FIGURE 4

A

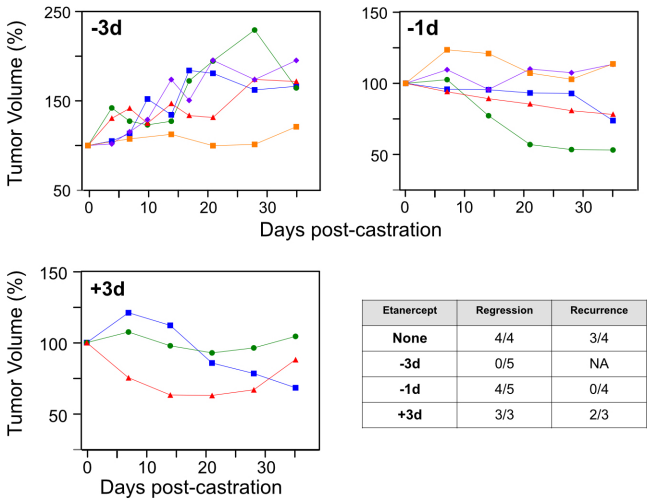

Etanercept	Regression	Recurrence
None	4/4	3/4
-3d	0/5	NA
-1d	4/5	0/4
+3d	3/3	2/3

B

Sham vs CX_6d

Genesets	SIZE	NES	p.val	FDR
PHONG_TNF_RESPONSE_VIA_P38_PARTIAL	144	-2.98	<0.01	5.16E-05
PHONG_TNF_RESPONSE_VIA_P38_COMPLETE	208	-2.94	<0.01	5.65E-05
RUAN_RESPONSE_TO_TNF_TROGLITAZONE_DN	39	-2.70	<0.01	2.97E-04
PHONG_TNF_TARGETS_UP	60	-2.65	<0.01	3.72E-04
RUAN_RESPONSE_TO_TNF_DN	80	-2.62	<0.01	4.81E-04
ZHOU_TNF_SIGNALING_30MIN	51	-1.97	<0.01	2.35E-02
ZHANG_RESPONSE_TO_IKK_INHIBITOR_AND_TNF_UP	190	-1.88	0.01	3.52E-02
ZHOU_TNF_SIGNALING_4HR	49	-1.85	0.01	4.09E-02
WANG_TNF_TARGETS	18	-1.77	0.02	5.82E-02
RUAN_RESPONSE_TO_TNF_TROGLITAZONE_UP	15	-1.68	0.03	8.09E-02

Sham vs CX_35d

Genesets	SIZE	NES	p.val	FDR
ZHANG_RESPONSE_TO_IKK_INHIBITOR_AND_TNF_UP	193	3.96	<0.01	9.35E-06
PHONG_TNF_TARGETS_UP	61	3.96	<0.01	9.35E-06
PHONG_TNF_RESPONSE_NOT_VIA_P38	307	3.72	<0.01	9.35E-06
WANG_TNF_TARGETS	19	3.5032	<0.01	9.35E-06
TIAN_TNF_SIGNALING_VIA_NFKB	27	3.2884	<0.01	9.35E-06
TIAN_TNF_SIGNALING_NOT_VIA_NFKB	21	2.7396	<0.01	1.64E-04
SANA_TNF_SIGNALING_UP	65	2.7088	<0.01	2.21E-04
PHONG_TNF_RESPONSE_VIA_P38_PARTIAL	149	2.3381	<0.01	2.27E-03
SANA_TNF_SIGNALING_DN	82	2.1602	<0.01	6.18E-03
ZHOU_TNF_SIGNALING_30MIN	51	1.8286	<0.01	3.32E-02
ZHOU_TNF_SIGNALING_4HR	49	1.7752	0.02	4.19E-02

Figure 4. Differentially-timed TNF signaling blockade has distinct effects on tumor growth. Mice with PTEN-deficient tumors were castrated and etanercept (sTNFR2-Fc) was administered at the indicated times: three days before (-3d), one day before (-1d), or three days after (+3d) surgical castration. **A.** Tumor volume kinetics. Tumor volumes were determined by serial HFUS imaging and 3D reconstruction and plotted after normalizing to the initial tumor volume for each mouse. Different colors/symbols represent individual mice. The table summarizes regression and recurrence incidence for each experiment. Growth curves for castrated mice that did not receive etanercept (None) are not shown. The criteria for regression and recurrence are described in the Materials and Methods. Statistical analysis is provided in Supplementary Table S3A. **B.** Gene set enrichment analysis. RNA was extracted from PTEN-deficient tumors from the following mice: sham-operated, 6d post-castration and 35d post-castration. GSEA was performed on bulk RNA-seq data using gene sets corresponding to TNF-related pathways. Normalized enrichment scores (NES) from RNA from tumors at 6d (down-regulated, blue) and 35d (up-regulated, red) post-castration were compared to the sham group. Gene sets common to the two analyses are highlighted in yellow.

FIGURE 5

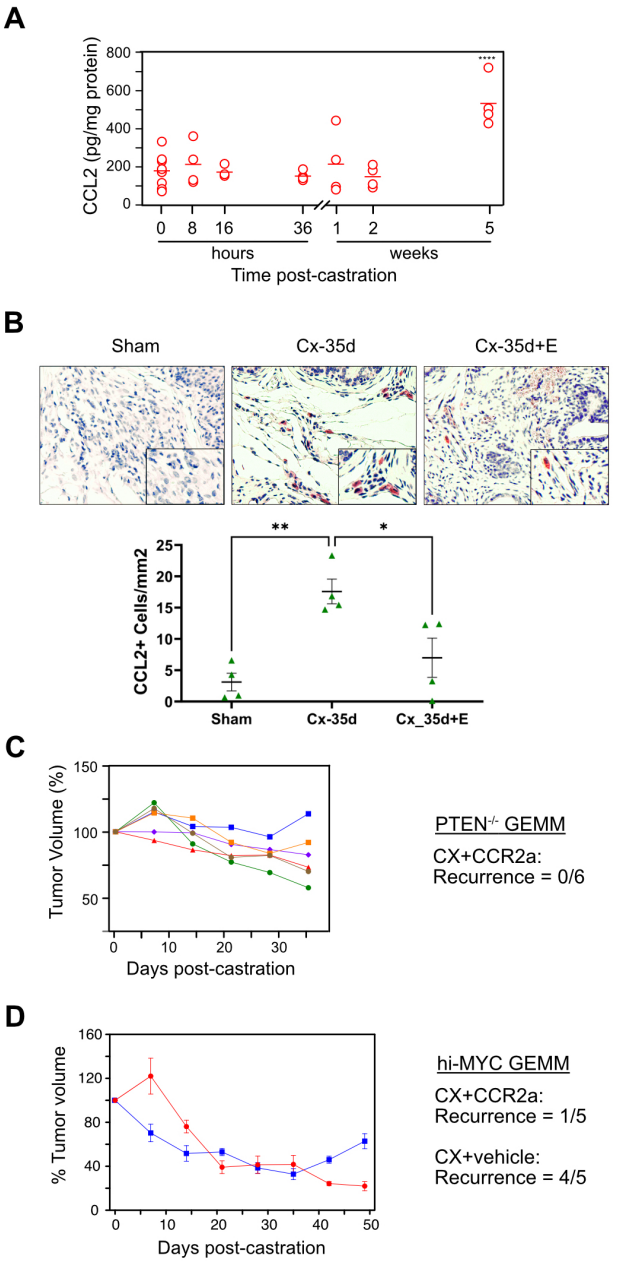

Figure 5. CCL2-CCR2 signaling is required for castration-resistant recurrence. Mice bearing PTEN-deficient (**A-C**) or hi-MYC (**D**) tumors were sham-operated or castrated at the indicated times. Volume was monitored by HFUS. Some mice received etanercept (E) or the CCR2a, as indicated. **A**. Tumor CCL2 levels following castration. CCL2 levels were measured by ELISA on the same tumor extracts prepared for Fig. 1C, normalized to total protein and plotted as open circles. The bar marks the mean. Two-way ANOVA followed by Tukey-Kramer HSD test revealed a difference in CCL2 levels between 0 and 5 weeks ($p < 0.0001$).(**B.** Representative images of IHC-stained $CCL2^+$ cells (red) in tumors from the indicated treatment groups. CCL2+ cells were counted and plotted. $^{**}p < 0.01$, $^{*}p < 0.05$ (Two-way ANOVA followed by Tukey-Kramer HSD test). **C.** Treatment with a CCR2 antagonist phenocopies -1d etanercept treatment (Fig. 4A) in PTEN-deficient tumor-bearing mice. Tumor volumes were determined by serial HFUS imaging and 3D reconstruction and plotted after normalizing to the initial tumor volume for each mouse (left). Different colors/symbols represent individual mice. The recurrence incidence is summarized (right). **D.** CCR2 antagonist suppresses castration-induced regression in Hi-MYC prostate cancer-bearing mice. Blue boxes: mice were castrated and received vehicle. Red circles: mice were castrated and received CCR2a prior to castration. N=5 for each group. The recurrence incidence is summarized (right). Tumor volume kinetics for individual mice are in Supplementary Figure S5. Statistical analysis for **C-D** is provided in Supplementary Table S3B.

FIGURE 6

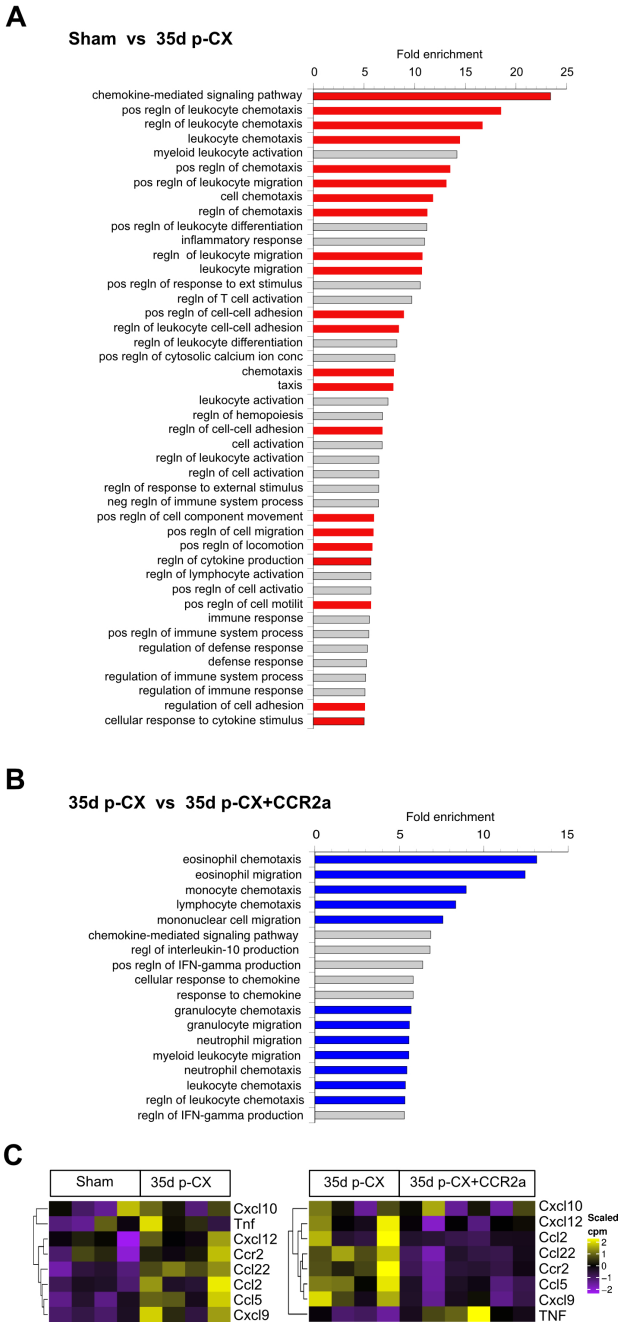

Figure 6. Transcriptomic changes in PTEN-deficient prostate cancers following CCL2 signaling blockade. RNA was extracted from PTEN-deficient tumors from the following mice: sham-operated (Sham), 35d post-castration (35d post-CX) and 35d post-castration after receiving CCR2a (35dp-CX+CCR2a). DGE analysis was performed on bulk RNAseq data (Fig. S6) followed by Gene Ontology analysis of biological processes comparing RNAseq transcript sets derived from tumors in mice that were sham-operated vs mice 35d post-castration (**A**) or from tumors in mice 35d post-castration vs mice treated with CCR2a 35d post-castration (**B**). Red-colored bars represent up-regulation and blue-colored bars represent down-regulation. Fold-enrichment >5. **C.** TAM-related transcripts regulated by CCL2 signaling. Heatmap representation of mRNA levels of select TAM-associated genes for the same two comparisons shown in **A** (left) and **B** (right).

FIGURE 7

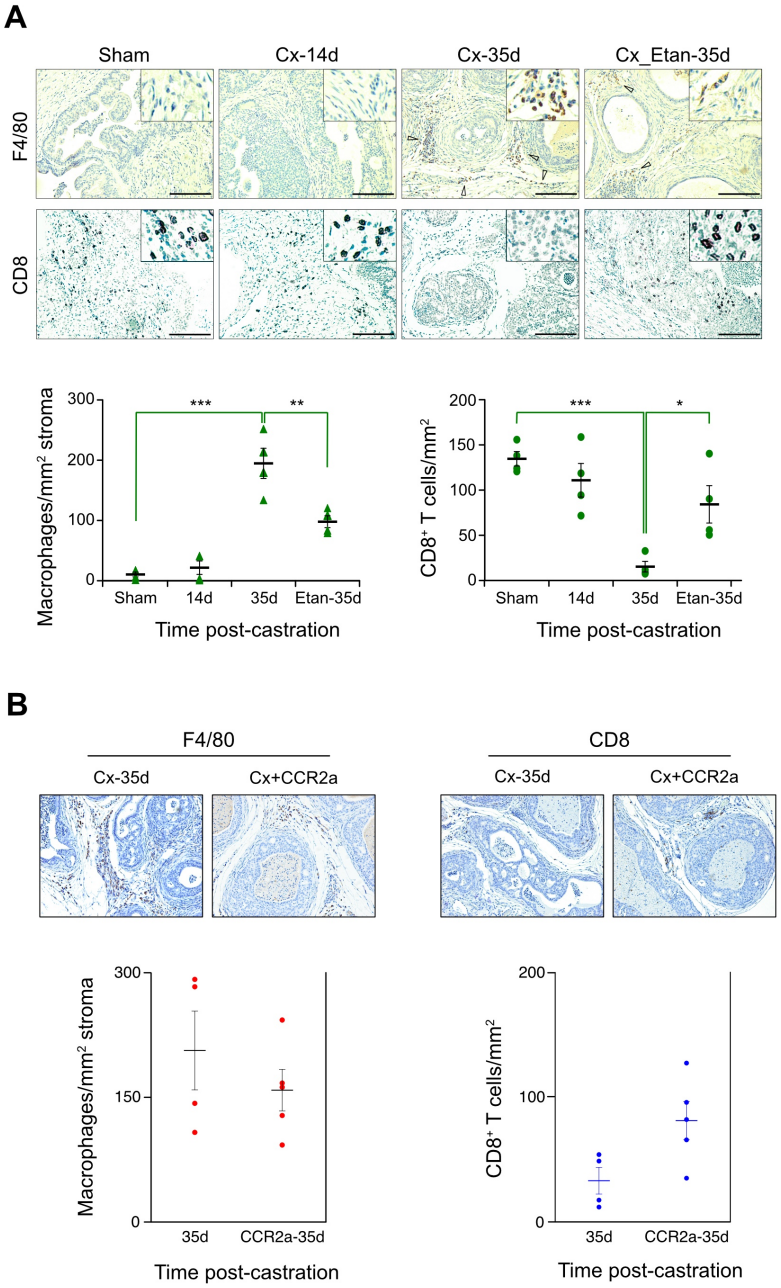

Figure 7. TNF and CCR2 signaling blockade suppress castration-induced immunosuppression at late times following castration. Mice bearing PTEN-deficient tumors were sham-operator or castrated (Cx) and tumors harvested at the indicated times post-castration. Some mice received etanercept (Etan) or the CCR antagonist BMS IHC staining for stromal F4/80+ macrophages and CD8+ T cells was performed and the number of stained cells per unit area were plotted. **A**. TNF signaling blockade. Images of representative IHC-stained tissue sections for the surface marker protein noted on the left side. Mice were treated as shown across top and the cell densities plotted for each of the treatments, below. **B**. CCL2 signaling blockade. Similar to **A** with both surface marker protein and corresponding mouse treatments shown along the top. A complete set of images are provided in Supplementary Figure S7C. Staining and counting of the Cx-35d samples in **A** and **B** were performed separately. Data are given as mean ± s.e.m. (n=4). *p<0.05, **p<0.01, ***p<0.001 (One-way ANOVA followed by Tukey-Kramer HSD test). *P*-value for the differences for CD8+ T cells and F4/80 macrophages due to CCR2a treatment was >0.05 (not statistically significant).

FIGURE 8

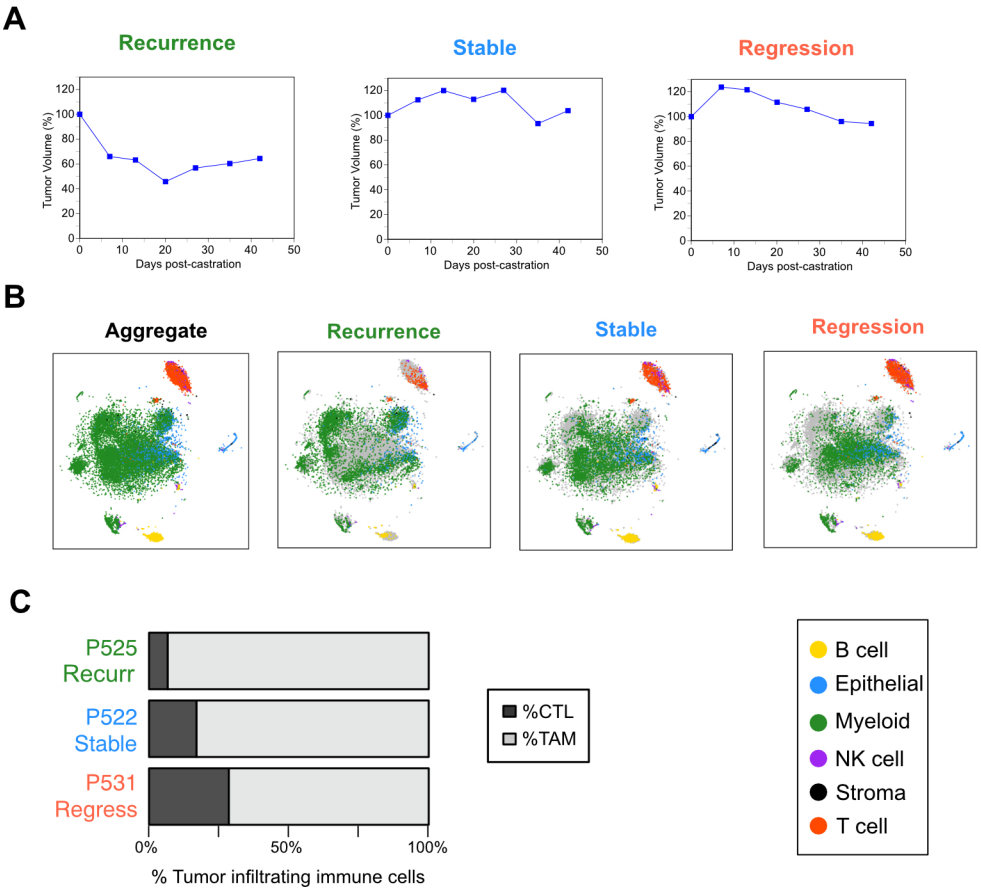

Figure 8. Tumor recurrence following castration correlates with an immunosuppressive tumor microenvironment. A. Post-castration tumor volume kinetics for three representative PTEN-deficient mouse tumors. Tumor volumes were determined by serial HFUS imaging and 3D reconstruction and plotted after normalizing to the initial tumor volume for each mouse. The average starting volume for these tumors was ~960 mm^3. **B.** t-SNE plots for single cell RNAseq analysis. At 42d post-castration, mice were sacrificed, tumor tissue was disaggregated into single cell preparations, RNA sequenced and analyzed as described in the Methods. Dimensionality reduction of cell transcriptomes from all three mice was performed with tSNE to produce the plot in far left panel (Aggregate). Cells are assigned to 6 subset populations as coded in the key in the lower right corner. Color-coded cells from each of the three mice corresponding to the response patterns in **A** are shown in the remaining three panels of **B**. Cells which were in the aggregate population, but not identified in individual mice are grey colored. TAMs (defined in panel C) are within the large, heterogeneous myeloid population (green). **C.** CTL:TAM ratios for regressing, stable or recurrent mouse tumors. Transcriptomic data from **B** was used to define TAMs (CD45 and CD68and CD80; lighter grey) and CTLs (CD45 and [CD3e or Cd3d or CD3g] and [CD8a or CD8b1]; darker grey). See text for discussion.